Adsorption of γ-Valerolactone: An Alternative for Solvent Recovery after Conversion of Lignocellulosic Biomass to Fermentable Sugars

L. G. Coelho,[a] G. Johann,[b,*] F. Palú,[a] M. G. A. Vieira,[c] R. Guirardello,[c] V. N. Trindade-Júnior,[d] and E. A. Silva[a]

[a]Chemical Engineering Course, Western State University of Paraná, Rua da Faculdade, 645, CEP 85903-000 Toledo, PR, Brazil

[b]Bioprocess Engineering and Biotechnology Course, Federal Technological University of Paraná, Estrada para Boa Esperança, Km 04, CEP 85660-000, Dois Vizinhos, PR, Brazil

[c]School of Chemical Engineering, State University of Campinas, Av. Albert Einstein, 500, CEP 13083-852, Campinas, SP, Brazil

[d]Federal University of Maranhão, DEQ, Av. dos Portugueses, 1966, Cidade Universitária Dom Delgado, CEP 65076-000, Sao Luis, MA Brazil

doi: https://doi.org/10.15255/CABEQ.2021.2009

Original scientific paper
Received: August 20, 2021
Accepted: June 10, 2022

The γ-valerolactone is an effective solvent in solubilizing lignocellulosic biomass fractions, although it inhibits microbial activity. To avoid the negative effects on the metabolism of microorganisms, even small quantities of γ-valerolactone need to be removed. This study examined the adsorption of γ-valerolactone on the commercial resin. The removal efficiency, adsorption equilibrium, pH effects, and fixed-bed column conditions were investigated. The highest removal efficiency of γ-valerolactone from sugar solution was 39.92 %, with 413.78 mg g^{-1} γ-valerolactone adsorption capacity, observed with commercial resin Dowex Optipore L-493 and pH 4.00. Dual-site Langmuir adsorption isotherm was found to be the best-fitting model for describing the adsorption mechanisms of γ-valerolactone on commercial resin. Thus, this study shows that γ-valerolactone could be removed from sugar solution by adsorption on commercial resin. In addition, the process is a viable alternative for the recovery of solvent and keeping the microbial activity in lignocellulosic biomass fractions.

Keywords:
commercial resin, separation, kinetic, equilibrium, batch, fixed-bed

Introduction

The growing demand for energy, as well as environmental issues have triggered the tendency to change the energy matrix. In 2018, 85.7 % of the world's energy was segmented by non-renewable sources. In Brazil, the scenario is quite different, in 2018, 54.7 % of the Brazilian energy matrix was composed of resources such as oil, gas, and coal[1]. This percentage difference is partially due to the use of biofuels as an alternative to fossil fuels. Numerous factors have caused the current trend toward production of biofuels using inedible raw materials, such as lignocellulosic. Lignocellulosic biomass, the annual production of which is 181.5 billion tonnes[2], is composed of cellulose, hemicellulose, and lignin, it has low cost, high availability, and carbohydrate content (>65 %)[3]. The production of essential products from lignocellulosic biomass, such as bioethanol, depends on its conversion into fermentable sugars[4], which should be simplified because it is step-demanding[5].

The conversion of lignocellulosic biomass to ethanol has four main steps: pretreatment, hydrolysis, fermentation, and product recovery. The pretreatment method depends on biomass type[6], and can improve the cost of bioethanol production[7]. Among the pretreatment methods, the use of organic solvents is a promising technique. There are various organic solvents used for the conversion of lignocellulosic biomass to fermentable sugars. Among them, γ-valerolactone (GVL) has been proven effective because it solubilizes all the lignocellulosic biomass fractions[8]. GVL is a renewable solvent derived from lignocellulosic biomass itself, is cheaper than enzymes, stable, biodegradable, and recyclable[9,10]. It allows high value-added materials to be produced, prevents solids from accumulating, and eliminates the filtration step[11].

*Corresponding author: E-mail: grajohann@gmail.com

Some studies evaluating the production of sugars[12–14] and alcohols[15–20] via a non-enzymatic route using GVL as a solvent are found in the literature. However, at high concentrations, as well as other organic solvents[21], GVL can inhibit the microorganisms responsible for fermentation. The subsequent recovery and reuse of GVL are significant regarding synthesis and process economy.

GVL has usually been separated using CO_2 extraction, which can remove up to 99.5 % of the solvent[13], and the residual amount of this solvent can be separated by adsorption. Nonetheless, only two studies on the adsorptive separation of GVL in aqueous glucose (GL) solution were found in the literature. In the first, the equilibrium isotherms for water and GL were evaluated, as well as the hydrolysis using GVL and commercial Amberlite XAD4®[22]. In the second, the particle diameter profile of the commercial resin Seapabeads SP850 was optimized for the adsorption of GVL from an aqueous solution containing GVL, GL, and xylose[23].

Therefore, the novelty of the present research is evaluation of an adsorption procedure for recovery of high quantities of γ-valerolactone from an aqueous GL solution. To achieve this main goal, equilibrium and kinetic data in a batch reactor and a fixed-bed reactor were provided, which are essential for designing the industrial-scale process. In terms of green engineering, the research promotes one crucial criterion: the recycling and reuse of a renewable solvent, which derives from lignocellulosic biomass and is cheaper than enzymes.

Experimental

Adsorptive capacity

The following commercial adsorbents were tested in the preliminary tests: activated carbon (Guaramex), organophilic clay (Spectrogel C), and four resins (Amberlite XAD16, Sepabeads SP825L, Sepabeads SP850, and Dowex Optipore L-493).

Aqueous solutions were prepared with GL and GVL, both by Sigma Aldrich, with 99 % purity, to evaluate the adsorptive capacity of six commercial adsorbents, as follows: [A] 24 g L^{-1} GVL and 66 g L^{-1} GL; [B] 12 g L^{-1} GVL and 33 g L^{-1} GL, which is the concentration obtained after the conversion of lignocellulosic biomass in the presence of the GVL solvent[24]. About 0.5 g of each adsorbent was added to the 25 mL of the solutions [A] and [B]. All flasks were placed in a cooled incubator and shaken at 100 rpm at 25 °C for 24 h (to ensure that the system reached equilibrium).

The equilibrium concentration in the resin was calculated as follows[25]:

$$q = \frac{(C_0 - C)V}{m} \quad (1)$$

where q is the adsorption capacity (mg g^{-1}), C_0 is the initial concentration (g L^{-1}), C is the final concentration of GVL in its fluid phase (g L^{-1}), V is the volume of the solution (L), and m is the mass of the resin (g).

Based on the results of the preliminary tests, one adsorbent was selected for a more detailed analysis, including its characterization, collection of equilibrium data at different pH values, and collection of breakthrough curves.

Having determined the material with higher adsorption capacity, it was characterized regarding humidity, actual density, and point of zero charge (pH_{pzc}). All determinations were made in duplicate.

Humidity was determined using an oven for 48 h at 70 °C until mass stability was achieved (until three consecutive weighings provided constant mass values). The actual density was measured using a gas pycnometer Micromeritics®, II AccuPyc 1340, belonging to the Laboratory of Engineering and Environmental Procedures (LAPA/FEQ/Campinas). The adsorbent was placed on the equipment at $1.35 \cdot 10^5$ Pa, 26.5 °C, 11.78 cm^3, at an equilibrium rate of $3.45 \cdot 10^2$ Pa min^{-1}. The evaluation of pH_{pzc} followed the method of Park and Regalbuto[26], using solutions with initial pH ranging from 1.00 to 11.00, 0.01 molar of NaCl, and 0.2 g of solid adsorbent. The flasks were shaken for 24 h at 100 rpm in the same equipment as used in the adsorptive capacity evaluation.

Batch adsorption equilibrium

The equilibrium tests were carried out using a shaking incubator. A solution of 25 mL containing water, GL, and GVL was placed in Erlenmeyer flasks. The initial concentration of GVL ranged between 13 and 80 g L^{-1}. The flasks were shaken for 24 h at 100 rpm. The experiment was performed in duplicate at different pH values: 2.00, 4.00, and 6.00. The equilibrium concentration in the resin was calculated using Eq. (1).

The Langmuir[27], Dual-site Langmuir[28], Freundlich[29], Sips[30], Redlich-Peterson[31], Toth[32], and Jovanovic[33] models were tested to describe the equilibrium relationship, as shown in Table 1.

In Table 1, q^* is the equilibrium adsorption capacity (mg g^{-1}), C^* is the equilibrium concentration (g L^{-1}), q_{max}, q_{m1}, q_{m2}, K_F, q_{mS}, q, q_{mT}, and q_{mJ} are the corresponding adsorption capacities for each isotherm (mg g^{-1}), b is the Langmuir isotherm constant (L g^{-1}), b_1 and b_2 are Dual-site Langmuir isotherm constants, nF is the Freundlich empirical parameter, BS and nS are Sips isotherm constants, BRP and

Table 1 – *Adsorption isotherm models*

Isotherm	Equation
Langmuir	$q^* = \frac{q_{max}\ b\ C^*}{1 + b\ C^*}$
Dual site Langmuir	$q^* = \frac{q_{m1}\ b_1\ C^*}{1 + b_1\ C^*} + \frac{q_{m2}\ b_2\ C^*}{1 + b_2\ C^*}$
Freundlich	$q^* = K_F C^{*nF}$
Sips	$q^* = \frac{q_{mS}\ BS\ C^{*nS}}{1 + BS\ C^{*nS}}$
Redlich-Peterson	$q^* = \frac{q\ BRP\ C^*}{1 + BRP\ C^{*nRP}}$
Toth	$q^* = \frac{q_{mT}\ KT\ C^*}{\left[1 + \left(KT\ C^*\right)^{nT}\right]^{1/nT}}$
Jovanovic	$q^* = q_{mJ}\left(1 - e^{BJ\ C^*}\right)$

Table 2 – *Operating conditions of column adsorption experiments*

Q (L min^{-1})	C_0 (g L^{-1})
1.7	27.65
1.7	22.79
1.7	18.21
1.7	13.59
1.7	8.44
2.7	17.93
3.7	17.84

nRP are Redlich-Peterson isotherm constants, *KT* and *nT* are Toth isotherm constants, and *BJ* is the Jovanovic isotherm constant.

The parameters of the equilibrium models were adjusted using the software Maple 16, through the NLPSolve routine. The minimized function was:

$$OBJ_{Eq} = \sum_{j=1}^{Ni}\left(q_{EXPj} - q_{CALj}\right)^2 \tag{2}$$

where OBJ_{Eq} is the objective function, Ni is the number of experimental data at a given temperature, q_{EXP} is the experimental concentration (mg g^{-1}), and q_{CAL} is the concentration calculated by the model (mg g^{-1}).

Kinetics of fixed-bed column adsorption

Continuous adsorption experiments were performed in a jacketed glass column, 20 cm in height and 0.9 cm internal diameter. The column was coupled to a thermostatic bath and a peristaltic pump to feed the solution. The previously treated and dried adsorbent was added to the column with distilled water. The column was fed with a solution containing water, GL, and GVL in upflow. Experiments were performed at different concentrations of GVL and flow, as shown in Table 2.

Experimental breakthrough curves determined the mass transfer zone parameters (*MTZ*):[25]

$$MTZ = L - L_u \tag{3}$$

where L is the total bed height (cm), and L_u is the useful length of the bed (cm), calculated as follows:[25]

$$L_u = \frac{q_{tb}}{q_{ts}} L \tag{4}$$

$$q_{tb} = \frac{QC_F}{m}\int_0^{t_b}\left(1 - \frac{C_{out}}{C_F}\right)dt \tag{5}$$

$$q_{ts} = \frac{QC_F}{m}\int_0^{t_s}\left(1 - \frac{C_{out}}{C_F}\right)dt \tag{6}$$

where q_{tb} is the amount of the adsorbate adsorbed per unit mass of adsorbent until the break point (mg g^{-1}), m is the mass of adsorbent in (g), t_b is the rupture time (min) corresponding to the time in which the ratio is $C_{out}/C_F = 0.05$, C_{out} is the GVL concentration in the outlet of the column (g L^{-1}), q_{ts} is the amount of adsorbate adsorbed per unit mass of adsorbent until the saturation time (mg g^{-1}), and t_s is the saturation time of the column (min), in which the ratio is $C_{out}/C_F = 1$.

To describe the column adsorption kinetics of GVL, the Bohart-Adams[34] model was used. This model considers that the adsorption rate can be represented by an irreversible second-order reaction rate model in the solid-fluid interface, represented by the following equations:

$$\frac{\partial C(t,z)}{\partial t} + \frac{\rho_b}{\varepsilon}\frac{\partial \overline{q}(t,z)}{\partial t} + v\frac{\partial C(t,z)}{\partial z} = 0 \tag{7}$$

$$\frac{\partial \overline{q}(t,z)}{\partial t} = k_a\left[q_t - \overline{q}(t,z)\right]C(t,z) \tag{8}$$

where t is the time (min), z is the spatial coordinate (m), ρ_b is the specific mass of the bed (g cm^{-3}), ε is the porosity of the bed, q_t is the experimental equilibrium concentration (mg g^{-1}), $\overline{q}$ is the average concentration of solute in the solid phase (mg g^{-1}), v is the interstitial velocity (cm min^{-1}), and k_a is the model kinetic constant (L g^{-1} min^{-1}).

The material balances are subject to the following initial and boundary conditions:

$$C(0, z) = 0 \tag{9}$$

$$\bar{q}(t,0)=0 \tag{10}$$

$$C(t,0)=\begin{cases}0, t=0\\ C_0, t>0\end{cases} \tag{11}$$

where C_0 is the feed concentration of the solute in the fluid phase (g L^{-1}).

The analytical solution of the Bohart-Adams model obtained by Amundson is[35]:

$$\frac{C_{out}}{C_0}=\begin{cases}0, t<t_f\\ \dfrac{1}{\left(e^{A}+e^{-B}-1\right)e^{B}}, t>t_f\end{cases} \tag{12}$$

where:

$$A=\frac{z\beta}{v}$$

$$B=\frac{(-tv+z)\beta}{\alpha v}$$

$$\propto=\frac{\rho_b q^*}{C_0\varepsilon}$$

$$\beta = k_a C_0 \infty$$

$$t_f=\frac{z}{v}$$

where C_{out} is the concentration of solute in the fluid phase in the outlet of the column (g L^{-1}), and t_f is the residence time of the adsorbate within the bed (min).

The Bohart-Adams model parameter was adjusted by the bisection method, using the Maple 16 software. The minimized function was:

$$OBF_K=\sum_{j=1}^{Ni}\left(C_{EXPj}-C_{CALj}\right)^2 \tag{13}$$

where OBF_K is the objective function used for estimation of the parameter of the Bohart-Adams model, Ni is the number of experimental data of the breakthrough curve, C_{EXP} is the experimental concentration (g L^{-1}), and C_{CAL} is the concentration calculated using the model (g L^{-1}).

Results and discussion

The experimental results of the adsorption capacity of the adsorbents tested (activated carbon, organophilic clay, Amberlite XAD16, Sepabeads SP825L, Sepabeads SP850, and Dowex Optipore L-493) are shown in Fig. 1.

Fig. 1 shows that the adsorbent with the highest adsorption capacity of GVL was the Dowex Optipore L-493 resin at both concentrations. Regarding this adsorbent, the adsorption capacity of GVL after the contact between the phases for 24 h was 413.78 and 304.71 mg g^{-1} for the solutions [A] and [B], respectively. The average removal using the L-493 resin was 3.48 % and 39.92 % for GL and GVL, respectively. Therefore, the L-493 resin was selected to study the kinetics and the adsorption of GVL in aqueous GL due to the interest in removing GVL and maintaining concentrations in the GL solution. After the characterization analyses of the L-493 resin, the values obtained were 4.30 % for humidity and 1.14 g cm^{-3} for density. Additional characterizations are available in the literature[36].

The pH_{pzc} was 4.00, a value in which the surface is considered neutral (i.e., below than this value the adsorbent surface has a net positive charge, and above this value results in the predominance of negative charges)[37]. Thus, the pH solution lower than 4.00 supports the adsorption of anions, while at higher pH, the adsorption of cations is favored due to the negative surface charge[38].

In this study, the models for obtaining the maximum adsorption capacity of GVL onto Dowex Optipore L-493 resin and information about the adsorption mechanism, given in Table 1, were evaluated. Table 3 presents the results obtained after adjusting the parameters of the isotherm models to the experimental data of the adsorption equilibrium of the solution containing GVL in contact with the resin.

Table 3 shows that all the equilibrium models presented an average correlation coefficient, $\bar{R}^2$, greater than or equal to 0.993 for all the pH conditions evaluated experimentally, indicating that all

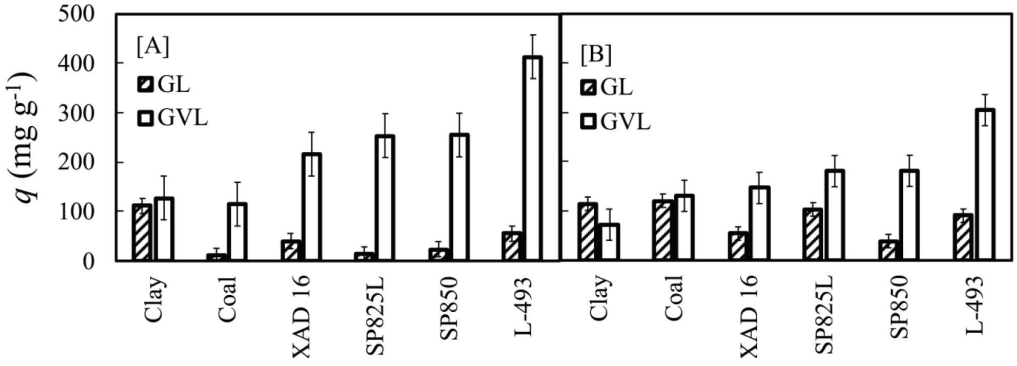

Fig. 1 – *Adsorptive capacity of the GVL by different adsorbents. [A] 24 g L^{-1} GVL and 66 g L^{-1} GL; [B] 12 g L^{-1} GVL and 33 g L^{-1} GL*

Table 3 – *Parameters set for the equilibrium isotherms*

Model	pH 2.00	pH 4.00	pH 6.00
Langmuir	$q_{max} = 413.40$ $b = 0.1970$	$q_{max} = 458.50$ $b = 0.1057$	$q_{max} = 435.99$ $b = 0.1596$
	$\overline{R}^2 = 0.999$ $\overline{ARE} = 8.79$ % $\overline{SSR} = 4627.586$		
Dual-site Langmuir	$q_{m1} = 710.92$ $b_1 = 0.0104$ $q_{m2} = 154.76$ $b_2 = 4.334$	$q_{m1} = 505.78$ $b_1 = 0.0203$ $q_{m2} = 139.60$ $b_2 = 1.351$	$q_{m1} = 435.99$ $b_1 = 0.1596$ $q_{m2} = 0$ $b_2 = 53.150$
	$\overline{R}^2 = 0.999$ $\overline{ARE} = 4.98$ % $\overline{SSR} = 1400.442$		
Freundlich	$K_F = 118.11$ $nF = 0.307$	$K_F = 94.51$ $nF = 0.363$	$K_F = 111.02$ $nF = 0.348$
	$\overline{R}^2 = 0.999$ $\overline{ARE} = 6.435$ % $\overline{SSR} = 1865.313$		
Sips	$q_{mS} = 2304.61$ $BS = 0.053$ $nS = 0.347$	$q_{mS} = 1841.65$ $BS = 0.051$ $nS = 0.426$	$q_{mS} = 442.97$ $BS = 0.164$ $nS = 0.347$
	$\overline{R}^2 = 0.999$ $\overline{ARE} = 5.13$ % $\overline{SSR} = 1515.103$		
Redlich-Peterson	$q = 118.12$ $BRP = 9748.25$ $nRP = 0.693$	$q = 96.097$ $BRP = 32.574$ $nRP = 0.641$	$q = 327.510$ $BRP = 0.248$ $nRP = 0.925$
	– 0.999 $\overline{ARE} = 5.17$ % $\overline{SSR} = 1428.578$		
Toth	$q_{mT} = 118.11$ $KT = 0$ $n = 1.44286$	$q_{mT} = 95.604$ $KT = 0.053$ $n = 1.563$	$q_{mT} = 297.364$ $KT = 4.462$ $n = 1.44286$
	$\overline{R}^2 = 0.999$ $\overline{ARE} = 5.14$ % $\overline{SSR} = 1420.150$		
Jovanovic	$_{mJ}$ 363.78 $bJ = 0.163$	$q_{mJ} = 295.43$ $bJ = 6.811$	$q_{mJ} = 268.55$ $bJ = 6.485$
	$\overline{R}^2 = 0.993$ $\overline{ARE} = 32.42$ % $\overline{SSR} = 46619.633$		

the models can be used to describe the equilibrium of the GVL solution with the Dowex Optipore L-493 resin. The best-fit order was Dual-site Langmuir > Sips > Toth > Redlich-Peterson > Freundlich > Langmuir > Jovanovic. The dual-site Langmuir model was slightly better than the other tested models, with the lowest sum of square residuals (*SSR*), and average relative error ($\overline{ARE}$), 4.98 % and 1400.442, respectively. Similar results were obtained in the adsorption of H_2S by waste oil fly ash[39,40].

Comparing the results from the Langmuir model and dual-site Langmuir model, it is clear that the first present almost twice the deviation of the second, 8.79 % (i.e, there are different binding sites in solid). The dual-site Langmuir assumes that the adsorption occurs in homogeneous and heterogeneous sites. Considering that its $\overline{R}^2$ was greater than or equal to 0.99, this ratifies the existence of two types of active sites (i.e., where chemisorption and physisorption is the predominant mechanism, respectively). For the dual-site Langmuir model, the calculated sorption capacity, q_{max}^{DS}, defined as the sum of saturation capacities, q_{m1} and q_{m2}, decreased with the increase in pH (865.68 to 435.99 mg g^{-1} for pH 2.00 to 6.00). In turn, the sorption affinities with binding sites, b_1 and b_2, increased with the pH.

The dimensionless parameters from the Langmuir isotherm, $R_L = 1/(1+C_0 b)$, indicates whether

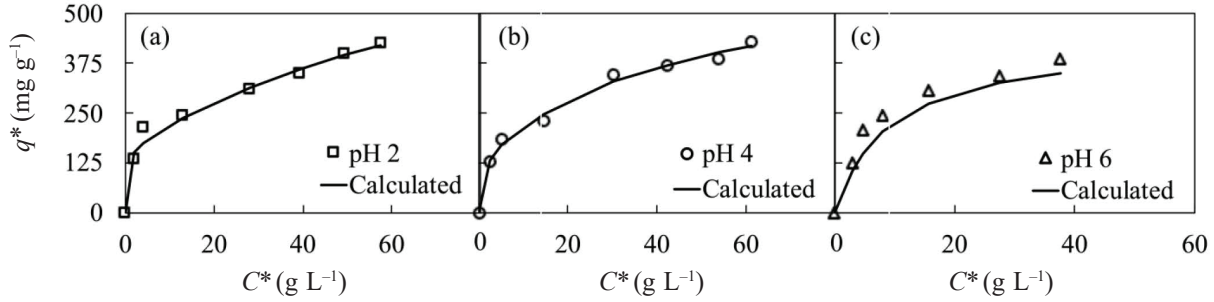

Fig. 2 – *Equilibrium data for pH 2 (a), 4 (b), and 6 (c)*

the adsorption is favorable or not. For the experimental results (Table 3), the R_L values were 0.72, 0.88, and 0.68, for pH 2.00, 4.00, and 6.00. Since all these values are in the range $0<R_L<1$, adsorption process is favorable[41]. In turn, from the Freundlich isotherm adjustment results, the adsorption intensity, *nF*, when less than unity, suggests that the adsorption is favorable. Also, a higher magnitude of the adsorption capacity, K_F, indicates relatively easy uptake at pH 2.00 as compared to 4.00 and 6.00[42,43].

The experimental values of the equilibrium data calculated by the dual-site Langmuir model are shown in Fig. 2, in which the higher the pH solution, the lower the adsorption capacity values of the isotherm in mg g^{-1}, as expected due to q_{max}^{DS} values.

Fig. 2 suggests that the adsorption of GVL on Dowex Optipore L-493 resin was unfavorable. The curves were concave and of type III, i.e., high concentrations of GVL are required for adsorption to be significant. This indicates that adsorption is sensitive to particle size since the effective adsorption area is highly influenced by the granulometry of the solid. This same behavior was noticed for the resin Seapabeads SP850 in adsorption of GVL from an aqueous solution containing GL and xylose, in which the particle diameter and output concentration were directly related[23]. Regardless, the adsorption of GVL onto Dowex Optipore L-493 resin was satisfactory since the experimental maximum adsorbed amounts were 424.56, 427.66, and 415.36 mg g^{-1}, respectively for pHs 2.00, 4.00, and 6.00 (i.e., adsorption was favored in acidic medium. The increase in pH solution above pH_{pzc} would turn the adsorbent surface negative, which would lead to a decline in GVL adsorption onto resin due to repulsive forces between phases[44].

For all the preliminary tests using the Tukey test at 5 % significance, no significant difference was observed between the adsorptive capacities obtained for the different pH values measured. This behavior shows that GVL is a stable ester and does not tend to dissociate, i.e., pH has no significant effect on the adsorption, unlike when the adsorbate has different ionic forms depending on the pH.

Considering the experimental results of the equilibrium curves in Table 3, and the fact that the natural pH of an aqueous solution of GVL and GL is 4.00 (experimentally determined range of pH_{pzc}), the fixed bed column adsorption kinetics were performed at pH 4.00. No adsorption competition for GL and GVL species was observed during the dynamic tests, and thus the mathematical model proposed, which considered monocomponent adsorption of the GVL, can be used to describe the process[45] . Based on experimental data, the removal efficiency was calculated, such as the rupture time and saturation time, t_b and t_s, the total adsorption and saturation capacities, q_{tb} and q_{ts}, the useful length of the bed, L_u, and the mass transfer zone, *MTZ*, were calculated. The results are shown in Table 4.

Table 4 – *Calculations of removal efficiency and operating parameters of the breakthrough curves*

Q (mL min^{-1})	C_0 (mg L^{-1})	Removal efficiency (%)	t_b (min)	t_s (min)	q_{tb} (mg g^{-1})	q_{ts} (mg g^{-1})	L_u (cm)	*MTZ* (cm)
1.7	27.65	74.17	24.89	33.55	142.90	192.66	14.46	5.04
1.7	22.79	78.76	43.41	55.11	247.21	313.86	15.36	4.14
1.7	18.21	77.43	33.55	43.33	188.46	243.39	14.94	4.35
1.7	13.59	74.10	41.63	56.18	239.89	323.73	14.59	5.10
1.7	8.44	69.57	50.84	73.08	282.03	405.40	13.01	5.69
2.7	17.93	63.60	19.94	31.35	182.25	286.54	12.08	6.91
3.7	17.84	57.36	12.41	21.64	148.09	258.18	10.89	8.10

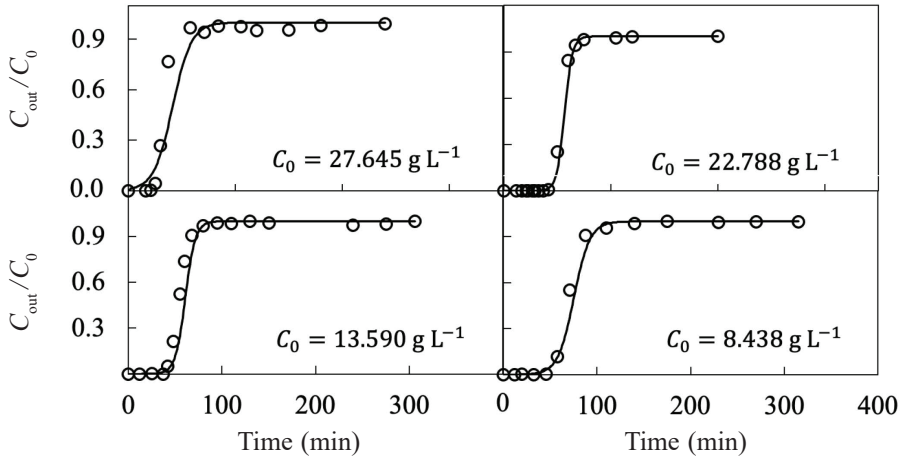

Fig. 3 – *Breakthrough curves at different concentrations*

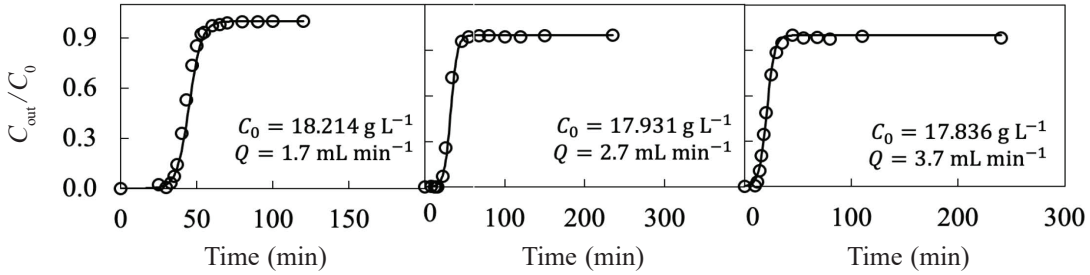

Fig. 4 – *Breakthrough curves for different ratios*

Traditional Bohart-Adams model[35] was employed to fit the breakthrough experimental data under different operating conditions. Figs. 3 and 4 show the experimental breakthrough curves calculated using the model, and Table 5 shows the values estimated for the kinetic constant k_a.

From Fig. 3 and Table 5, the slope of the breakthrough curve and the kinetic constant, k_a were directly influenced by the feed concentration, C_0. The highest concentration of GVL in the feed, 27.65 mg L^{-1}, was accompanied by a higher slope and rupture time reduced to 60 min. For this run, the kinetic constant k_a was the lowest, 0.00412 L g^{-1} min^{-1}, so the high GVL concentration provided the higher driving force, and the mass transfer overcame the resistance. In other words, the greater the C_0, the higher the gradient $\left(q_t - \overline{q}\right)$, and consequently, the mass transfer was faster. Thus, the better performance was a consequence of the steeper curve[46]. As expected, the average concentration of solute in the solid phase was directly proportional to C_0.

The order of magnitude obtained for the kinetic constant was similar to those observed in the adsorption of other organic compounds, such as phenolic compounds in apple juice[47], and the total organic carbon in water affected by the oil sand process[48]. For the constant flow of a solution containing water, GL, and GVL, the increase in feed concentration (C_0 from 8.44 to 27.65 g L^{-1}) decreased the kinetic constant (k_a from 0.01386 to 0.00412 L g^{-1} min^{-1}). Regarding constant feed concentration, about 18 g L^{-1}, the increase in flow rate (Q from 1.7 to 3.7 L min^{-1}) was accompanied by the increase in the value of (k_a from 0.01194 to 0.01556 L g^{-1} min^{-1}). Both these results may indicate that the organic material adsorption is controlled by external mass transfer resistance in the initial zone of adsorption in the fixed-bed column[49], in accordance with the good Bohart-Adams model agreement.

Fig. 4 shows that, at constant feed concentration, the breakthrough developed faster with increasing flow rate. As the flow rate was increased from 1.7 to 3.7 mL min^{-1}, the exhaust time (corresponding to 98 % of influent concentration) was found to decrease from 62 to 46 min. At the same

Table 5 – *Parameters estimated for the Bohart-Adams model*

Q (L min^{-1})	C_0 (g L^{-1})	k_a (L g^{-1} min^{-1})	R^2
1.7	27.65	0.00412	0.928
1.7	18.21	0.01194	0.991
1.7	22.79	0.01353	0.986
1.7	13.59	0.01360	0.955
1.7	8.44	0.01386	0.986
2.7	17.93	0.01360	0.993
3.7	17.84	0.01556	0.996

time, the rupture, t_b, and saturation, t_s, times, the mass ratio adsorbed until breakpoint, q_{tb}, and the useful length of the bed, L_u, had reduced. This occurred because increasing the flow rate reduces the contact time between phases, which decreases the mass transfer between them and the removal efficiency. These results agree with those from Table 4, where the greatest efficiency in the removal of GVL was 78.76 %, obtained for the run with 1.7 min^{-1} and 22.79 mg L^{-1}, which presented the lowest *MTZ*, 4.14 cm. The GVL uptake capacity was also influenced by the flow rate, as it increased from 1.7 to 3.7 mL min^{-1}, and the amount of total GVL uptake (**q_{tb}** from Table 4) reduced from 188.46 to 148.09 mg g^{-1}.

In the present study, different adsorbent masses and column lengths were not evaluated due to technical issues. However, as observed in the equilibrium isotherms (Fig. 2), more available areas are expected to increase the column's saturation time. However, indiscriminately increasing the column's length is not indicated, since the access to the binding sites could be restricted at higher bed heights due to axial dispersion, channeling, and bed compaction[50].

In Figs. 3 and 4, and Table 5, the R^2 average value was 0.976 for all the conditions measured, indicating closeness between the values of solute concentration in the fluid phase obtained experimentally and calculated by the Bohart-Adams model. Especially in the early stages of adsorption, the model underestimated the breakthrough curve values. This occurs due to the increased availability of the solvent to be captured by the adsorbent in the early stages and because the model considers only the average concentration values, reducing the driving force for mass transfer in the calculations. The good agreement of deep bed kinetics by the Bohart-Adams model implies that the surface diffusion is the rate-controlling step for adsorption of GVL in GL solution[51].

Conclusions

In this study, GVL was recovered by adsorption from GL solution. The process was investigated in batch experiments and packed columns. In preliminary tests for the evaluation of different adsorbents in the removal of GVL from solution, the L-493 resin presented the highest efficiency. The pH had no influence on adsorption of GVL, so the use of the natural value of the aqueous solution was proposed for this adsorption process. The experimental equilibrium data were best fitted by the dual-site Langmuir model, suggesting the existence of two types of active sites. Packed column experiments showed that the adsorption process was unfavorable, controlled by external resistance, and satisfactory. The Bohart-Adams model suitably described the breakthrough curves. The column adsorption process was found to perform better at higher influent GVL concentration and lower flow rate. Finally, the commercial resin can be efficiently applied to recover GVL remained in a sugar solution with highly efficient removal, promoting the environmentally friendly process of conversion of cellulose and hemicellulose into fermentable sugars without inhibition.

Nomenclature

b	–	Langmuir isotherm constant
BJ	–	Jovanovic isotherm constant
BRP	–	Redlich-Peterson isotherm constant
BS	–	Sips isotherm constant
b_1	–	Dual-site Langmuir isotherm constant
b_2	–	Dual-site Langmuir isotherm constant
C	–	Final concentration in fluid phase, g L^{-1}
C_{CAL}	–	Concentration calculated using the model, g L^{-1}
C_{EXP}	–	Experimental concentration, g L^{-1}
C_{out}	–	Concentration in the outlet of the column, g L^{-1}
C_0	–	Initial concentration in fluid phase, g L^{-1}
C^*	–	Equilibrium concentration in fluid phase, g L^{-1}
k_a	–	Model kinetic constant, L g^{-1} min^{-1}
K_F	–	Adsorption capacity, mg g^{-1}
KT	–	Toth isotherm constant
L	–	Total bed height, cm
L_u	–	Useful length of the bed, cm
m	–	Mass of the resin, g
MTZ	–	Mass transfer zone
nF	–	Freundlich empirical parameter
Ni	–	Number of experimental data
nRP	–	Redlich-Peterson isotherm constant
nS	–	Sips isotherm constant
nT	–	Toth isotherm constant
OBJ_{Eq}	–	Objective function
OBF_K	–	Objective function
q	–	Adsorption capacity, mg g^{-1}
$\overline{q}$	–	Average concentration of solute in the solid phase, mg g^{-1}
q_{EXP}	–	Experimental concentration, mg g^{-1}
q_{CAL}	–	Concentration calculated by the model, mg g^{-1}
q_{max}	–	Adsorption capacity, mg g^{-1}
q_{mJ}	–	Adsorption capacity, mg g^{-1}
q_{mS}	–	Adsorption capacity, mg g^{-1}
q_{mT}	–	Adsorption capacity, mg g^{-1}
q_{m1}	–	Adsorption capacity, mg g^{-1}

q_{m2} – Adsorption capacity, mg g^{-1}
q_t – Experimental equilibrium concentration calculated, mg g^{-1}
q_{tb} – Amount of adsorbate, mg g^{-1}
q_{ts} – Amount of adsorbate until the saturation time, mg g^{-1}
q^* – Equilibrium adsorption capacity, mg g^{-1}
t – Time, min
t_b – Rupture time, min
t_f – Residence time, min
t_s – Saturation time of the column, min
v – Interstitial velocity, cm min^{-1}
V – Volume of the solution, L
z – Spatial coordinate, m
ρ_b – Specific mass of the bed, g cm^{-3}
ε – Porosity of the bed

ACKNOWLEDGEMENTS

This study was financed in part by the Coordenação de Aperfeiçoamento de Pessoal de Nível Superior – Brasil (CAPES) – Finance Code 001.

References

1. *Ministério de Minas e Energia*, Published online 2019 (2019).
2. *Tisma, M.*, *Bucic-Kojic, A.*, *Planinic, M.*, Bio-based products from lignocellulosic waste biomass: A state of the art, Chem. Biochem. Eng. Q. **35** (2021) 139. doi: https://doi.org/10.15255/CABEQ.2021.1931
3. *Shin, G. J.*, *Jeong, S. Y.*, *Lee, J. W.*, Evaluation of antioxidant activity of the residues generated from ethanol concentration of lignocellulosic biomass using pervaporation, J. Ind. Eng. Chem. **52** (2017) 51. doi: https://doi.org/10.1016/j.jiec.2017.03.023
4. *Cho, E. J.*, *Song, Y.*, *Lee, Y. J.*, *Bae, H. J.*, Preparation and characterization of novel green magnetic nanocatalyst for cellulosic biomass degradation under mild conditions, J. Ind. Eng. Chem. **40** (2016) 185. doi: https://doi.org/10.1016/j.jiec.2016.06.022
5. *Tao, C.*, *Peng, L.*, *Zhang, J.*, *He, L.*, Al-modified heteropolyacid facilitates alkyl levulinate production from cellulose and lignocellulosic biomass: Kinetics and mechanism studies, Fuel Process. Technol. **213** (2021) 1. doi: https://doi.org/10.1016/j.fuproc.2020.106709
6. *Kumar, B.*, *Bhardwaj, N.*, *Agrawal, K.*, *Chaturvedi, V.*, *Verma, P.*, Current perspective on pretreatment technologies using lignocellulosic biomass: An emerging biorefinery concept, Fuel Process. Technol. **199** (2020) 1. doi: https://doi.org/10.1016/j.fuproc.2019.106244
7. *Inan, B.*, *Özçimen, D.*, A comparative study of bioprocess performance for improvement of bioethanol production from macroalgae, Chem. Biochem. Eng. Q. **33** (2019) 133. doi: https://doi.org/10.15255/CABEQ.2018.1499
8. *Wu, P.*, *Li, L.*, *Sun, Y.*, *Song, B.*, *Yu, Y.*, *Liu, H.*, Near complete valorisation of Hybrid pennisetum to biomethane and lignin nanoparticles based on gamma-valerolactone/water pretreatment, Bioresour. Technol. **305** (2020) 1. doi: https://doi.org/10.1016/j.biortech.2020.123040
9. *Kondeboina, M.*, *Enumula, S. S.*, *Gurram, V. R. B.*, *Chada, R. R.*, *Burri, D. R.*, *Kamaraju, S. R. R.*, Selective hydrogenation of biomass-derived ethyl levulinate to γ-valerolactone over supported Co catalysts in continuous process at atmospheric pressure, J. Ind. Eng. Chem. **61** (2018) 227. doi: https://doi.org/10.1016/j.jiec.2017.12.020
10. *Zhu, J.-Q.*, *Wu, X.-L.*, *Li, W.-C.*, *Qin, L.*, *Chen, S.*, *Xu, T.*, *Liu, H.*, *Zhou, X.*, *Li, X.*, *Zhong, C.*, *Li, B.-Z.*, *Yuan, Y.-J.*, Ethylenediamine pretreatment of corn stover facilitates high gravity fermentation with low enzyme loading, Bioresour. Technol. **267** (2018) 227. doi: https://doi.org/10.1016/j.biortech.2018.07.030
11. *Alonso, D. M.*, *Wettstein, S. G.*, *Dumesic, J. A.*, Gamma-valerolactone, a sustainable platform molecule derived from lignocellulosic biomass, Green Chem. **15** (2013) 584. doi: https://doi.org/10.1039/C3GC37065H
12. *Luterbacher, J. S.*, *Rand, J. M.*, *Alonso, D. M.*, *Han, J.*, *Youngquist, J. T.*, *Maravelias, C. T.*, *Pfleger, B. F.*, *Dumesic, J. A.*, Nonenzymatic sugar production from biomass using biomass-derived γ-valerolactone, Science **343** (2014) 277. doi: https://doi.org/10.1126/science.1246748
13. *Shuai, L.*, *Questell-Santiago, Y. M.*, *Luterbacher, J. S.*, A mild biomass pretreatment using γ-valerolactone for concentrated sugar production, Green Chem. **18** (2016) 937. doi: https://doi.org/10.1039/C5GC02489G
14. *Li, S. X.*, *Li, M. F.*, *Yu, P.*, *Fan, Y. M.*, *Shou, J. N.*, *Sun, R. C.*, Valorization of bamboo by γ-valerolactone/acid/water to produce digestible cellulose, degraded sugars and lignin, Bioresour. Technol. **230** (2017) 90. doi: https://doi.org/10.1016/j.biortech.2017.01.041
15. *Al-Shaal, M. G.*, *Wright, W. R. H.*, *Palkovits, R.*, Exploring the ruthenium catalysed synthesis of γ-valerolactone in alcohols and utilisation of mild solvent-free reaction conditions, Green Chem. **14** (2012) 1260. doi: https://doi.org/10.1039/C2GC16631C
16. *Han, J.*, *Luterbacher, J. S.*, *Alonso, D. M.*, *Dumesic, J. A.*, *Maravelias, C. T.*, A lignocellulosic ethanol strategy via nonenzymatic sugar production: Process synthesis and analysis, Bioresour. Technol. **182** (2015) 258. doi: https://doi.org/10.1016/j.biortech.2015.01.135
17. *Kong, X.*, *Xu, H.*, *Wu, H.*, *Wang, C.*, *He, A.*, *Ma, J.*, *Ren, X.*, *Jia, H.*, *Wei, C.*, *Jiang, M.*, *Ouyang, P.*, Biobutanol production from sugarcane bagasse hydrolysate generated with the assistance of gamma-valerolactone, Process Biochem. **51** (2016) 1538. doi: https://doi.org/10.1016/j.procbio.2016.06.013
18. *Li, H.*, *Fang, Z.*, *Yang, S.*, Direct catalytic transformation of biomass derivatives into biofuel component γ-valerolactone with magnetic nickel-zirconium nanoparticles, ChemPlusChem. **81** (2016) 135. doi: https://doi.org/10.1002/cplu.201500492
19. *Trevorah, R. M.*, *Huynh, T.*, *Vancov, T.*, *Othman, M. Z.*, Bioethanol potential of Eucalyptus obliqua sawdust using gamma-valerolactone fractionation, Bioresour. Technol. **250** (2018) 673. doi: https://doi.org/10.1016/j.biortech.2017.11.084
20. *Byun, J.*, *Han, J.*, Environmental analysis of bioethanol production strategies from corn stover via enzymatic and nonenzymatic sugar production, Bioresour. Technol. **328** (2021) 1. doi: https://doi.org/10.1016/j.biortech.2021.124808
21. *Kaur, P.*, *Kocher, G. S.*, *Taggar, M. S.*, Development of fungal consortium for the pretreatment of rice straw under optimized solid state and shake flask conditions, Environ. Prog. Sustain. Energy **38** (2019) 635. doi: https://doi.org/10.1002/ep.12954

22. *Trindade-Junior, V. N.*, *Luterbacher, J. S.*, *Dumesic, J. A.*, *Silva, E. A.*, *Guirardello R.*, Adsorption of water/glucose mixture onto Amberlite resin, Chem. Eng. Trans. **43** (2015) 607.
doi: https://doi.org/10.3303/CET1543102
23. *Soeiro, T. N.*, *Guirardello, R.*, Optimization of the particle diameter profile in a fixed bed for separation of γ-valerolactone, Chem. Eng. Trans. **65** (2018) 583.
doi: https://doi.org/10.3303/CET1865098
24. *Trindade Júnior, V. N.*, Analysis of the separation processes in the production of cellulosic ethanol a starting from biomass by non-enzymatic route, Doctoral Thesis (2015).
25. *Worch, E.*, Adsorption Technology in Water Treatment: Fundamentals, Processes, and Modeling, De Gruyter, Germany, 2012.
26. *Park, J.*, *Regalbuto, J.*, A simple, accurate determination of oxide PZC and the strong buffering effect of oxide surfaces at incipient wetness, J. Colloid Interface Sci. **175** (1995) 239.
doi: https://doi.org/10.1006/jcis.1995.1452
27. *Langmuir, I.*, The constitution and fundamental properties of solids and liquids, J. Am. Chem. Soc. **38** (1916) 2221.
doi: https://doi.org/10.1021/ja02268a002
28. *Mathias, P. M., Kumar, R., Moyer, J. D., Schork, J. M., Srinivasan, S. R., Auvil, S. R., Talu, O.*, Correlation of multicomponent gas adsorption by the dual-site Langmuir model. Application to nitrogen/oxygen adsorption on 5A-zeolite, Ind. Eng. Chem. Res. **35** (1996) 2477.
doi: https://doi.org/10.1021/ie950291y
29. *Freundlich, H.*, Über die adsorption in lösungen, Z. Phys. Chem. **57U** (1907) 385.
doi: https://doi.org/10.1515/zpch-1907-5723
30. *Sips, R. J.*, On the structure of a catalyst surface, J. Chem. Phys. **16** (1948) 490.
doi: https://doi.org/10.1063/1.1746922
31. *Redlich, O.*, *Peterson, D. L.*, A Useful adsorption isotherm, J. Phys. Chem. **63** (1959) 1024.
doi: https://doi.org/10.1021/j150576a611
32. *Toth, J.*, State equations of the solid gas interface layer, Acta Chim. Acad. Sci. Hung. **69** (1971) 311.
33. *Jovanovic, D. S.*, Physical adsorption of gases, II: Practical application of derived isotherms for monolayer and multilayer adsorption, Colloid Polym. Sci. **235** (1969) 1214.
doi: https://doi.org/10.1007/BF01542531
34. *Bohart, G. S.*, *Adams, E. Q.*, Some aspects of the behavior of charcoal with respect to chlorine, J. Am. Chem. Soc. **42** (1920) 523.
doi: https://doi.org/10.1021/ja01448a018
35. *Amundson, N. R.*, A note on the mathematics of adsorption in beds, J. Phys. Colloid Chem. **52** (1948) 1153.
doi: https://doi.org/10.1021/j150463a007
36. *Liu, S., Huang, W., Shu, W., Li, Z., Goodman, B. A., Tan, X., Diao, K.*, Performance of L-493 macroprous resin for adsorption of trihalomethanes from water, Water Air. Soil. Pollut. **229** (2018).
doi: https://doi.org/10.1007/s11270-018-3898-7
37. *Ur, Rehman, M. Z.*, *Aslam, Z.*, *Shawabkeh, R. A.*, *Hussein, I. A.*, *Mahmood, N.*, Concurrent adsorption of cationic and anionic dyes from environmental water on amine functionalized carbon, Water Sci. Technol. **81** (2020) 466.
doi: https://doi.org/10.2166/wst.2020.119
38. *Pant, B. D., Neupane, D., Paudel, Lohani, P. C., Gautam, S. K., Pokhrel, M. R., Poudel, B. R.,* Efficient biosorption of hexavalent chromium from water by modified arecanut leaf sheath, Heliyon **8** (2022) e09283.
doi: https://doi.org/10.1016/j.heliyon.2022.e09283
39. *Aslam, Z.*, *Hussein, I. A.*, *Shawabkeh, R. A.*, *Parvez, M. A.*, *Ahmad, W.*, *Ihsanullah*, Adsorption kinetics and modeling of H_2S by treated waste oil fly ash, J. Air Waste Manag. Assoc. **69** (2019) 246.
doi: https://doi.org/10.1080/10962247.2018.1536004
40. *Aslam, Z.*, Carbonaceous adsorbent from waste oil fly ash: Surface treatments and hydrogen sulfide adsorption potential, Chem. Pap. (2022).
doi: https://doi.org/10.1007/s11696-022-02182-4
41. *Chand, A.*, *Chand, P.*, *Khatri, G. G.*, *Paudel, D. R.*, Enhanced removal efficiency of arsenic and copper from aqueous solution using activated acorus calamus based adsorbent, Chem. Biochem. Eng. Q. **35** (2021) 279.
doi: https://doi.org/10.15255/CABEQ.2021.1943
42. *Zahir, A.*, *Aslam, Z.*, *Aslam, U.*, *Abdullah, A.*, *Ali, R.*, *Bello, M. M.*, *Paspalum notatum* grass-waste-based adsorbent for rhodamine B removal from polluted water, Chem. Biochem. Eng. Q. **34** (2020) 93.
doi: https://doi.org/10.15255/CABEQ.2020.1830
43. *Aslam, Z.*, *Yousaf, I.*, *Akhtar, A.*, *Zahi, A.*, Adsorptive performance of MWCNTs for simultaneous cationic and anionic dyes removal; kinetics, thermodynamics, and isotherm study, Turkish J. Chem. **45** (2021) 1189
doi: https://doi.org/10.3906/kim-2005-12
44. *Naseem, S., Aslam, Z., Abbas, A., Sumbal, S. Ali, R., Usman, M.*, Synthesis and application of cobalt-based metal-organic framework for adsorption of humic acid from water, Chem. Biochem. Eng. Q. **36** (2022) 39.
doi: https://doi.org/10.15255/CABEQ.2021.1960
45. *Sağ, Y.*, *Ataçoğlu, I.*, *Kutsal, T.*, Simultaneous biosorption of chromium(VI) and copper(II) on *Rhizopus arrhizus* in packed column reactor: Application of the competitive Freundlich model, Sep. Sci. Technol. **34** (1999) 3155.
doi: https://doi.org/10.1081/SS-100100828
46. *Aslam, Z.*, *Anait, U.*, *Abbas, A.*, *Ihsanullah, I.*, *Irshad, U.*, *Mahmood, N.*, Adsorption of carbon dioxide onto activated carbon prepared from lawn grass, Biomass Conv. Bioref. (2020).
doi: https://doi.org/10.1007/s13399-020-01029-w
47. *Kibar, E. A. A.*, Adsorptive recovery of phenolics from apple juice via batch and fixed bed column, J. Food. Eng. **239** (2018) 114.
doi: https://doi.org/10.1016/j.jfoodeng.2018.07.005
48. *Niasar, H. S.*, *Das, S.*, *Xu, C. (C.)*, *Ray, M. B.*, Continuous column adsorption of naphthenic acids from synthetic and real oil sands process-affected water (OSPW) using carbon-based adsorbents, Chemosphere **214** (2019) 511.
doi: https://doi.org/10.1016/j.chemosphere.2018.09.078
49. *Aksu, Z.*, *Gönen, F.*, Biosorption of phenol by immobilized activated sludge in a continuous packed bed: Prediction of breakthrough curves, Process. Biochem. **39** (2004) 599.
doi: https://doi.org/10.1016/S0032-9592(03)00132-8
50. *Franco, M. A. E.*, *Carvalho, C. B.*, *Bonetto, M. M.*, *Soares, R. P.*, *Féris, L. A.*, Diclofenac removal from water by adsorption using activated carbon in batch mode and fixed-bed column: Isotherms, thermodynamic study and breakthrough curves modeling, J. Clean. Prod. **181** (2018) 145.
doi: https://doi.org/10.1016/j.jclepro.2018.01.138
51. *Ahmed, M. J.*, *Hameed, B. H.*, Removal of emerging pharmaceutical contaminants by adsorption in a fixed-bed column: A review, Ecotoxicol. Environ. Saf. **149** (2018) 257.
doi: https://doi.org/10.1016/j.ecoenv.2017.12.012